Available online at www.sciencedirect.com

SciVerse ScienceDirect

Ceramics International 39 (2013) 5013–5024

CERAMICS INTERNATIONAL

www.elsevier.com/locate/ceramint

Divalent silver oxide-diatomite hybrids: Synthesis, characterization and antibacterial activity

Wenning Shen[a,*], Lajun Feng[a], Hui Feng[b], Ali Lei[a]

[a]School of Materials Science and Engineering, Xi'an University of Technology, no. 5 South Jinhua Road, Xi'an 710048, China
[b]Shaanxi Institute of Zoology, Xi'an 710032, China

Received 14 August 2012; received in revised form 28 November 2012; accepted 29 November 2012
Available online 12 January 2013

Abstract

To produce better antibacterial and low water-soluble submicron powders of divalent silver oxide (AgO), divalent silver oxide-diatomite (AgO-d) hybrids were studied. AgO-d hybrids were prepared by chemical oxidation, using silver nitrate and diatomite as raw materials and potassium persulfate as oxidant. The results show that AgO-d hybrids with AgO weight percentage up to 20.8% are obtained by oxidation of Ag^+ adsorbing on diatomite in alkaline solution ($n(KOH)/n(AgNO_3)=7.5$) for 1.5 h at 333.15 K. Products were characterized by laser particle sizer, SEM, XRD, XPS, FT-IR and atomic absorption spectrophotometer (AAS). AgO-d hybrids are composed of tetragonal cristobalite, amorphous silica, monoclinic divalent silver oxide and a few of cubic silver oxide. Element Ag can be released from AgO-d hybrids but the dissolution speed is slow, which is about 3.20×10^{-2} mg (L h)$^{-1}$. Antibacterial effectiveness of AgO-d hybrids was tested against *Staphylococcus aureus* (*S. aureus* ATCC6538) and *Escherichia coli* (*E. coli* ATCC8099) by the shake-flask method. Results show that AgO-d hybrids possess excellent antibacterial properties. When the concentration of AgO-d hybrids is 10 mg L^{-1} and the contact time with *S. aureus* and *E. coli* is 30 min, the bactericidal rates reach up to 99.974% and 99.944%, respectively.

Keywords: D. AgO; D. Diatomite; E. Antibacterial; B. XPS

1. Introduction

Silver or silver ions have long been known to have strong inhibitory and bactericidal effects without any toxic effect [1–3]. They can inhibit the growth of various microorganisms, including bacteria [4,5], molds [6], yeasts [7], fungi [8–10] and viruses [11,12]. Recently, due to the growing applications of microbial resistance in commonly used antibiotics, intensive studies have been made to the bactericidal activities of silver nanoparticles [13,14], silver nanoparticle-based materials [15–17], silver containing composites [18–20], as well as silver oxides and ultrafine AgO powder-based materials [21–24]. The antibacterial activity of silver-containing compounds has been widely used to reduce infections in burn treatment [25] and arthroplasty [26] to prevent bacteria colonization on prostheses [27], catheters [28], and human skin [29], as well as to purify and improve water quality [2]. High-valence silver oxides such as AgO possess better bactericidal effect [30]. Shen et al. [31] have found that the antibacterial effectiveness of submicron AgO was higher than that of Ag_2O of submicron size. Lalueza et al. [32] have tested the bactericidal effect of different materials and the result showed that their effect is ordered in the following sequence: $AgNO_3$ > Ag-ZSM-5 > Ag_2O > commercial silver-exchanged zeolite (granular) > commercial silver-exchanged zeolite (pellets) > Ag nanoparticles. Moreover, the antimicrobial activity of AgO is influenced by the dimension of the particles, with smaller particles showing greater antimicrobial effect [33].

Therefore, in developing the route of synthesis, an emphasis was made to control the size of AgO particles. However, submicron and nano-scale powders alone in solution easily aggregate, resulting in deterioration of their chemical properties, a loss of their antibacterial properties

*Corresponding author. Tel.: +86 29 8231 2733, +86 13152075522; fax: +86 29 8231 2733.
E-mail addresses: shenwenning@qq.com (W. Shen), fenglajun@xaut.edu.cn (L. Feng).

0272-8842/$ - see front matter
http://dx.doi.org/10.1016/j.ceramint.2012.11.099

and the difficulty of recovery [24,34]. To solve these problems we grafted AgO submicron particles onto diatomite particles using a modified chemical oxidation method. Diatomite particles can provide high surface area and high absorbability for silver ion sorption, give excellent mechanical strength for supporting AgO submicron particles, offer thermal and chemical stability, and are inexpensive [35,36]. Diatomite has been used previously to grow TiO_2 NPs for improving photo catalytic properties of TiO_2 and diatomite composites [37,38]. Rastogi et al. [39] have prepared Ag–SiO_2 composites on a core of silica NPs functionalized with ethylenediamino-propyltrimethoxysilane and improved antibacterial properties of Ag and SiO_2 composites.

In our study silver nitrate and diatomite were used as precursors to develop low-cost, poor water-soluble, easily recovered and highly-efficient AgO-d antibacterial materials for improving water quality and recycling use. Thus, we grafted AgO ultrafine particles with strongly absorbing diatomite particles by chemical oxidation method and studied their antibacterial activity against *E. coli* and *S. aureus* in aqueous culture media.

2. Material and methods

2.1. Materials

Diatomite (chemical purity, Tianjin Tianda Chemical Reagent Plant), $AgNO_3$ (analytical purity, Xi'an Nonferrous Metals Research Institute), $K_2S_2O_8$ and KOH (analytical purity, Tianjin Tianli Chemical Reagent Co., Ltd.) were used as reactants for the synthesis of AgO-d hybrids. $MnSO_4$ (analytical purity, Tianjin Taixing Reagent Factory), H_3PO_4 (analytical purity, Chengdu Kelong Chemical Reagent Factory), $(NH_4)_2Fe(SO_4)_2 \cdot 6H_2O$ (analytical purity, Tianjin Tianhe Chemical Reagent Factory), and $C_{13}H_{11}NO_2$ (analytical purity, Chengdu Jinshan Chemical Reagent Factory) were employed to test the content of AgO in AgO-d hybrids. Deionized water was self-made in the laboratory.

2.2. Synthesis of AgO-d hybrids

AgO-d hybrids were synthesized by chemical oxidation method. Specifically, diatomite was washed with deionized water to remove fines and other adhered impurities, then calcined in a muffle furnace at 823.15 K for 2 h, and cooled naturally in the furnace to room temperature. 25 mL of $AgNO_3$ solutions with concentrations of 0.5, 1.0, 1.5 2.0 and 2.5 mol L^{-1} were prepared. 10 g of calcined diatomite was separately immersed in the $AgNO_3$ solutions for 96 h at room temperature, in order to allow Ag^+ to be fully absorbed onto the diatomite. After that, diatomite was separated with the $AgNO_3$ solutions by centrifugation. Then 100 mL of $K_2S_2O_8$ solution and 50 mL of KOH solution were prepared. The molar ratios of $K_2S_2O_8$ to $AgNO_3$ was 3:1 and that of KOH to $AgNO_3$ were 5:1, 6:1, 7:1, 7.5:1 and 8:1 respectively. Subsequently, the prepared aqueous solution of $K_2S_2O_8$ was transferred to a 500 mL glass round-bottomed flask fitted with a stirrer, a glass funnel for introducing diatomite adsorbing Ag^+ and a separating funnel to introduce the aqueous solution of KOH. The flask was then placed in a thermostat water bath at 323.15–363.15 K. The separated diatomite adsorbing Ag^+ was then added into the aqueous solution of $K_2S_2O_8$ under vigorous stirring for 2 min. And then, the KOH solution was added drop-wise to the reaction solution. The product solution was vigorously stirred for a specified time (0.5–2.5 h). After the specified time, oxidation was discontinued, the solid product was collected and the pH value of the reaction solution was tested by a PHS-25 acidimeter. The solid product was then washed repeatedly with deionized water until the product became neutral, and was dried at 343.15 K for 8 h.

2.3. AgO mass content test of AgO-d hybrids

The mass contents of AgO in AgO-d hybrids were determined, according to Mn^{2+} oxidation–reduction method. The measuring principle of AgO mass content is

$$AgO + Mn^{2+} + 2H^+ = Ag^+ + Mn^{3+} + H_2O \tag{1}$$

The general procedure used to measure the mass content of AgO was as follows. A 0.1 g tested sample was mixed with 10 mL of 5% (w/v) manganese sulfate solution and 10 mL of 25% (v/v) phosphoric acid, stirred with a magnetic stirrer for 10 min. The solution was titrated with standard ammonium ferrous sulfate solution with the concentration of 0.028 mol L^{-1} until the reaction solution revealed light red color. A drop of phenyl anthranilic acid indicator was added, and the titration was discontinued when the color became light yellow. The volume required to titrate was recorded. The mass content of AgO was estimated from the equation [40]

$$\omega(AgO) = \frac{0.028 \times V \times 123.83}{1000m} \times 100\% \tag{2}$$

where V is the consumed volume of the standard ammonium ferrous sulfate solution (mL), and m is the mass of the AgO-d hybrids sample (g).

2.4. Characterization

2.4.1. Size distribution analysis

The particle size, size distribution of calcined diatomite and AgO-d hybrids were measured by a BT-2003 laser particle sizer. Before testing, ultrasonic pretreatment was used to disperse samples, and deionized water was used as a testing medium.

2.4.2. AAS

The release property of AgO-d hybrids in solutions was studied using a TAS-986 atomic absorption spectrophotometer (AAS). The test procedure was as follows. Each AgO-d hybrid sample of 0.05 g was immersed in 200 mL of deionized water for 6, 12, 18, 24 and 30 days respectively. The solutions were then filtrated and the contents of element Ag in the filtrates were determined by AAS. The acquisition parameters were set as follows: detection wavelength of 328.1 nm, slit width of 0.4 nm, height and location of the atomizer of 6.0 and −1.0 mm respectively, the flow rate of propane of 2500 mL min^{-1}.

2.4.3. XRD

The crystal structure and phase composition of calcined diatomite and AgO-d hybrids were analyzed by an XRD-7000S X-ray diffractometer (XRD). XRD data were collected at room temperature with an X-ray source of Cu X-rays ($\lambda=0.15418$ nm). Additional acquisition parameters were: tube voltage, 40 kV; tube current, 30 mA; 2θ range, 20°–80°; and scan speed, 10° min^{-1}.

2.4.4. XPS

The surface chemical component and element quantivalency of calcined diatomite and AgO-d hybrids were studied using X-ray photoelectron spectroscopy (XPS). The XPS spectra were obtained using a Kratos Axis Ultra instrument, which is equipped with an analytical chamber of base pressure $\sim 10^{-9}$ Torr, a dual anode X-ray source (Mg/Al), and a hemispherical electron energy analyzer. Spectra were excited using monochromatic AlKα (150 W, 15 kV, 1486.7 eV). The pass energy was set to 50 eV for wide scanning and 20 eV for narrow scanning. Binding energies were calibrated relatively to the C1s peak ($E_b=284.8$ eV) from hydrocarbons adsorbed on the surface of the samples.

2.4.5. FT-IR

The changes of chemical structure of calcined diatomite and AgO-d hybrids were analyzed by an FT-IR-Prestige 21 Fourier transform infrared spectrometer (FT-IR). Acquisition parameters were: range = 400–4000 cm^{-1} and resolution = 2 cm^{-1}. Samples were analyzed by using the KBr disk technique.

2.4.6. SEM

An AMRAY MODEL 1000 scanning electron microscope (SEM) was used to scan the surface morphologies of raw diatomite and calcined diatomite at an accelerating voltage of 30 kV. The morphology of AgO-d hybrids was examined using a JSM-6700F scanning electron microscope equipped with an Oxford INCA X-ray energy dispersive spectroscope (EDS) at an accelerating voltage of 10 kV and an accelerating current of 10 μA. For the SEM analysis, the insulating sample was coated with a thin film of Pt, and the chemical compositions of raw diatomite, calcined diatomite and AgO-d hybrids were analyzed by EDS.

2.5. Measurement of bactericidal activity

S. aureus (ATCC6538) and *E. coli* (ATCC8099) are used as Gram-positive and Gram-negative bacteria respectively. The bacteria cultures were incubated at 310.15 K in beef extract-peptone medium (3 g of beef extract, 10 g of peptone, 15 g of sodium chloride, 20 g of agar, and 1000 mL of water). The concentrations of the bacteria were controlled from 1×10^6 to 9×10^6 CFU mL^{-1}. AgO-d hybrids suspensions with the concentrations of 10, 30, 70 and 112 mg L^{-1} were mixed thoroughly with *S. aureus* and *E. coli* solutions respectively. Then the mixtures were oscillated for 30 min and dropped into the beef extract-peptone medium at 318.15 K. Finally, the mixtures were incubated on a rotary shaker at 310.15 K for 48 h. The bactericidal effects of AgO-d hybrids were estimated from the equation:

$$X=\frac{A-B}{A}\times 100\% \tag{3}$$

where X is the bactericidal rate of AgO-d hybrids (%), A is the average count of bacterial colonies of control group without bactericide, and B is the average count of bacterial colonies of AgO-d hybrids samples tested.

3. Results and discussion

3.1. Analysis of the physical property of diatomite

3.1.1. Chemical compositions of raw and calcined diatomite

The chemical compositions of raw and calcined diatomite were analyzed by EDS. As shown in Table 1, raw diatomite consists of element Si (27.15%), O (70.65%), Mg (0.47%), Na (1.36%) and Cl (0.37%). After washing and being calcined at 823.15 K for 2 h, element Mg and Na had disappeared from diatomite, and the amounts of element Si and O increased. This indicates that the purity of raw diatomite has been improved after washing and calcine treatments.

Table 1
Chemical composition of raw diatomite and calcined diatomite (%).

Element	Si	O	Mg	Na	Cl
Atomic percentage					
Raw diatomite	27.15	70.65	0.47	1.36	0.37
Calcined diatomite	27.62	71.95	0	0	0.43

3.1.2. Morphology analysis

SEM micrographs of raw and calcined diatomite are shown in Fig. 1. As shown in Fig. 1(a), raw diatomite was nearly discoid in shape with a diameter of ~40 μm. Many impurities were adhered onto the surface of raw diatomite and most of the pores were blocked. After being calcined at 823.15 K, most deposited impurities were burnt off. Many subcircular pores were observed in calcined diatomite with a diameter of ~470 nm.

3.2. Potassium persulphate-mediated synthesis of AgO-d hybrids

3.2.1. Effect of $AgNO_3$ concentration

Table 2 shows the effect of $AgNO_3$ (Ag^+) concentration on the content of AgO (Ag^{2+}) in different AgO-d hybrids. The content of AgO in the hybrids increased with concentration of $AgNO_3$. The growth rate of AgO by weight in the hybrids increased rapidly with $AgNO_3$ concentration below 2.0 mol L^{-1}, but tend to be stable over 2.0 mol L^{-1}. That is to say, the adsorption amount of Ag^+ in diatomite increased with the concentration of $AgNO_3$ increasing, then became stable over 2.0 mol L^{-1}. This indicates that the adsorption amount of Ag^+ in diatomite has a critical value at 2.0 mol L^{-1} of $AgNO_3$.

3.2.2. Effect of initial reaction temperature

AgO-d hybrids, which were prepared with 1.5 mol L^{-1} $AgNO_3$ at different temperatures, 323.15 K, 333.15 K, 343.15 K, 353.15 K and 363.15 K, were used to investigate the effect of initial reaction temperature on the content of AgO.

From Table 3, it can be seen that initial reaction temperature had a critical influence on the content of AgO in the hybrids. From 323.15 K to 333.15 K, the content of AgO increased with initial reaction temperature. However, above 333.15 K, the content of AgO decreased. Since the oxidation of Ag^+ by $S_2O_8^{2-}$ is an exothermic reaction [41], the released heat increases the temperature and accelerates the reaction speed. When the initial temperature reaches to 333.15 K, or more, the reaction releases a lot of heat. The released heat cannot be diffused in time, so the reaction favors the direction of gaining heat, i.e., the dissolution of AgO, which will result in a decrease in AgO formation.

3.2.3. Effect of reaction time

Table 4 shows the effect of reaction time on the content of AgO in the hybrids. The content of AgO first increased, and then decreased with time. This result indicates that the oxidation of Ag^+ adsorbed onto diatomite might be completed in 1.5 h. The stability of diatomaceous SiO_2 in solution is affected by the pH value of reaction solution. When the pH value is less than 11, SiO_2 does not dissolve. However, the solubility of SiO_2 increases obviously when the pH value is over 12 [42]. The pH value of the reaction solution for preparing AgO-d hybrids was 13.47, being strongly alkaline. Thus, the OH^- added firstly neutralized H^+ produced by the oxidation of Ag^+ by $S_2O_8^{2-}$ in 1.5 h, and it had not enough time to react with SiO_2. When the reaction time was over 1.5 h, the produced H^+ was total neutralized. Since the pH value of the reaction solution was over 13, SiO_2 would react with OH^- and AgO to form silicate, leading to the decrease in AgO content.

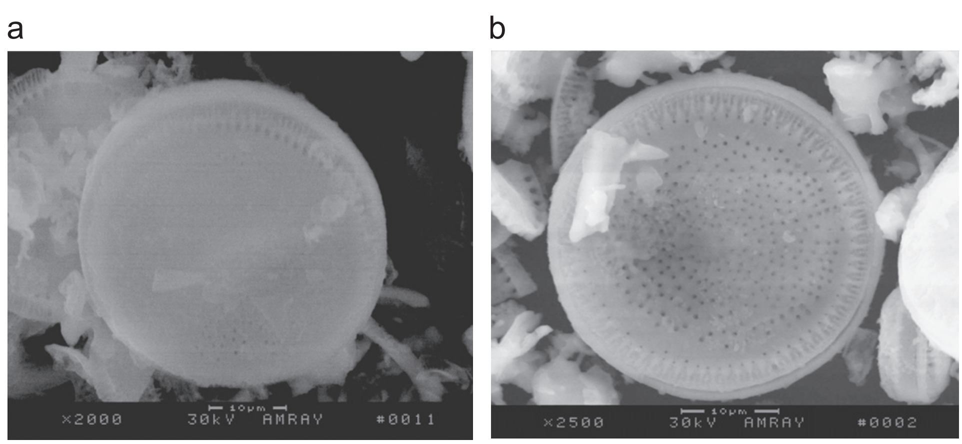

Fig. 1. SEM morphologies of raw diatomite and calcined diatomite. (a) Raw diatomite, 2000 times and (b) diatomite calcined at 823.15 K, 2500 times.

Table 2
Effects of $AgNO_3$ concentration on the AgO content of AgO-d hybrids (333.15 K, $n(KOH)/n(AgNO_3)=7.5$, 1.0 h).

$C(AgNO_3)$ (mol L^{-1})	0.5	1.0	1.5	2.0	2.5
Adsorption amount of Ag^+ in diatomite (mol)	0.0051	0.0106	0.0159	0.0228	0.0249
ω_{AgO} (%)	5.39	9.44	13.32	16.48	18.61

Table 3
Effects of initial reaction temperature on the AgO content of AgO-d hybrids ($C(AgNO_3)=1.5\ mol\ L^{-1}$, $n(KOH)/n(AgNO_3)=7.5$, 1.0 h).

Initial reaction temperature (K)	323.15	333.15	343.15	353.15	363.15
ω_{AgO} (%)	8.64	13.35	12.23	10.98	7.65

Table 4
Effects of reaction time on the AgO content of AgO-d hybrids ($C(AgNO_3)=1.5\ mol\ L^{-1}$, $n(KOH)/n(AgNO_3)=7.5$, 333.15 K).

Reaction time (h)	0.5	1	1.5	2	2.5
ω_{AgO} (%)	10.58	17.86	19.08	15.52	5.20

Table 5
Effects of KOH concentration on the AgO content of AgO-d hybrids ($C(AgNO_3)=1.5\ mol\ L^{-1}$, 333.15 K, 1.0 h).

$n(KOH)/n(AgNO_3)$	5	6	7	7.5	8
pH value after reaction	8.11	9.24	13.55	13.71	13.42
ω_{AgO} (%)	1.21	1.91	17.34	17.86	13.27

3.2.4. Effect of KOH concentration

Table 5 shows the effect of KOH concentration on the weight percentage of AgO in the hybrids. The content of AgO was influenced by the concentration of KOH solution. For $n(KOH)/n(AgNO_3)=5$–6, the weight percentage of AgO was low and increased slowly. For $n(KOH)/n(AgNO_3)>6$, the weight percentage of AgO increased apparently and then decreased. The pH value of the solution after the reaction first increased, and then decreased with the increasing KOH concentration.

The results suggest that the formation of AgO into diatomite was likely to be affected by the competing precipitation-dissolution processes of AgO and the dissolution of SiO_2. When $n(KOH)/n(AgNO_3)$ value is lower than 6, the pH value of reaction solution is low, the dissolution rate of AgO is greater than the precipitation rate of AgO, which results in the low weight percentage of AgO. However, for $n(KOH)/n(AgNO_3)=6$–7.5, the H^+ generated by oxidation of Ag^+ can be neutralized timely and AgO precipitation is the main reaction. Consequently, the weight percentage of AgO increases quickly. But further increase of KOH concentration may cause a strong alkalinity of the solution, resulting in the formation of colloidal silicate through the reaction of SiO_2 and AgO with KOH. The colloidal materials can block the pores of diatomite and prevent further oxidation of Ag^+, which decreases the percentage of AgO.

Based on the above analysis, the optimum conditions for the preparation of AgO-d hybrids with the maximum content of AgO, 20.8%, were as follows: $AgNO_3$ concentration of $2.0\ mol\ L^{-1}$, initial reaction temperature of 333.15 K, reaction time of 1.5 h and $n(KOH)/n(AgNO_3)$ value of 7.5. The prepared AgO-d hybrids were used for further characterization and testing.

3.3. Physical properties of AgO-d hybrids

Table 6 is the size distribution and particle size of calcined diatomite and AgO-d hybrids. The size distribution of calcined diatomite was in the range 0.685–180.4 μm, and the median size was 26.73 μm. After the deposition of AgO, the size distribution was in the range 0.614–116.5 μm, and the median size decreased to 18.53 μm. Compared with calcined diatomite, the particle size distribution of AgO-d hybrids became narrower and the mean particle size became smaller. It may be caused by two reasons. One is that the volume expansion of AgO grain formation by oxidation of Ag^+ adsorbed on diatomite and the volume expansion of grain growth caused diatomite particle crush. The other is that diatomite particles are cracked by strong mechanical agitation.

The stability of the hybrids in solution was investigated by immersing 0.05 g of AgO-d hybrids in 200 mL deionized water for 6, 12, 18, 24 and 30 days. The silver dissolved quantity from AgO-d hybrids was tested by AAS and the result is shown in Table 7. It can be seen that element Ag can be released from AgO-d hybrids in solution. Silver dissolved quantity in the solution was observed to increase with the immersing time. After immersing for 30 days, the concentration of element Ag was $23.0\ mg\ L^{-1}$ and its releasing rate was about $3.20\times10^{-2}\ mg\ (L\ h)^{-1}$, calculated through one-dimensional linear regression equation. This indicates that AgO-d hybrids have silver dissolved ability, and the dissolution rate is slow, which is beneficial to save the bactericide. As reported by Antelman [43], silver dissolution reaction from AgO-d hybrids in solution may be presented as follows,

$$AgO+H_2O=Ag^{2+}+2OH^- \quad (4)$$

3.4. Crystal structure and chemical composition

3.4.1. XRD analysis

Fig. 2 shows the XRD patterns of calcined diatomite and AgO-d hybrids. The typical XRD pattern of calcined diatomite shows that diffraction peaks at 21.774°, 28.326°, 31.147°,

Table 6
Size distributions of calcined diatomite and AgO-d hybrids obtained by oxidation of Ag^{+} adsorbed onto diatomite (immersing in $AgNO_3$ solution of 2.0 mol L^{-1}, $n(KOH)/n(AgNO_3)=7.5$, 333.15 K, 1.5 h). (μm).

Samples	Size distribution	Median size	Bulk mean size	Area mean size
Calcined diatomite	0.685–180.400	26.730	34.093	12.527
AgO-d hybrids	0.614–116.500	18.530	22.613	9.845

Table 7
Silver dissolved amount of AgO-d hybrids obtained by oxidation of Ag^{+} adsorbed onto diatomite (immersing in $AgNO_3$ solution of 2.0 mol L^{-1}, $n(KOH)/n(AgNO_3)=7.5$, 333.15 K, 1.5 h).

Immersing time (days)	6	12	18	24	30
Concentration of element Ag (mg L^{-1})	4.58	9.23	13.65	18.48	23.00

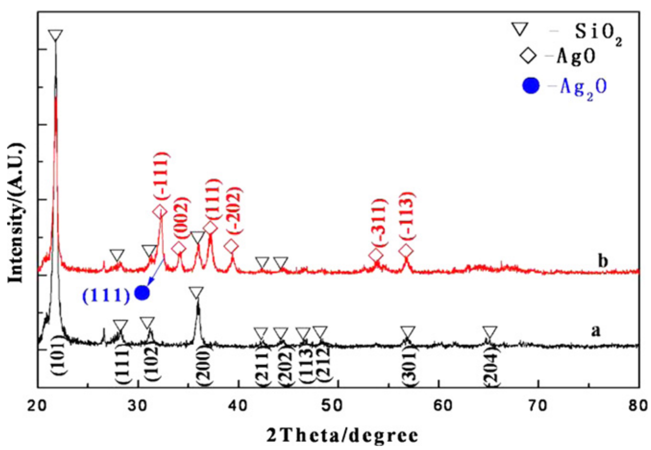

Fig. 2. XRD patterns of calcined diatomite and AgO-d hybrids obtained by oxidation of Ag^{+} adsorbed onto diatomite (immersing in $AgNO_3$ solution of 2.0 mol L^{-1}, $n(KOH)/n(AgNO_3)=7.5$, 333.15 K, 1.5 h). (a) Calcined diatomite and (b) AgO-d hybrids.

35.967°, 42.389°, 44.526°, 46.868°, 48.461°, 56.815° and 65.041° can be indexed to the (101), (111), (102), (200), (211), (202), (113), (212), (301) and (204) planes of low cristobalite. This indicates that calcined diatomite is of crystallinity, and the crystal structure belongs to tetragonal system. After the deposition of AgO, there are diffraction peaks at 21.782°, 28.189°, 31.183°, 35.972° and 46.809° in the XRD pattern of AgO-d hybrids, corresponding to low cristobalite. Compared with calcined diatomite, the diffraction peak positions for low cristobalite of AgO-d hybrids did not shift significantly, but the peaks at 42.389°, 44.526°, 48.461°, 56.815° and 65.041° disappeared. This indicates that the deposition of AgO did not change the phase composition and crystal structure of diatomite. Moreover, the silver oxides might be deposited on the pores and surface, and block the pores of diatomite. Sequentially, some weak peaks disappeared. Besides, several diffraction peaks of AgO-d hybrids appear at 32.254°, 34.154°, 37.240°, 39.407°, 53.786° and 56.736° in the XRD pattern corresponding to diffraction crystal faces of AgO (−111), (002), (111), (−202), (−311) and (−113). The diffraction peak at 32.702° in the XRD pattern may refer to the crystal face of Ag_2O (111), but the other three strong diffraction peaks of Ag_2O did not appear. This indicates that element Ag of AgO-d hybrids exists in the form of AgO and litter Ag_2O after deposition, and the crystal structures of AgO and Ag_2O belong to the monoclinic system and cubic system, respectively.

3.4.2. XPS analysis

The chemical compositions of calcined diatomite and AgO-d hybrids were determined by survey XPS spectra (Fig. 3). The elemental composition of calcined diatomite was Si(15.32%), O(42.40%), C(40.29%) and Na(1.99%), and that of AgO-d hybrids was Si(7.84%), O(35.14%), C(49.42%), Na(0.76%) and Ag(6.84%). The carbon impurity might be resulted from the adsorption of residual hydrocarbons in the UHV chamber of the XPS instrument, or CO_2 from air.

As shown in Fig. 4, information about the electronic states of silicon in calcined diatomite and AgO-d hybrids can be deduced from high-resolution XPS spectra. The Si2p spectrum of calcined diatomite contains two distinct peak maxima. There must be two electronic states of silicon existing. The peak at 102.5 eV is in excellent agreement with XPS data of amorphous silica [44]. And the other peak at 103.25 eV agrees well with cristobalite reported in the Handbook of X-Ray Photoelectron Spectroscopy [45]. After being deposited with AgO, the Si2p spectra of AgO-d hybrids still contain two peaks, and the relevant binding energies are 102.5 eV and 103.25 eV respectively. This indicates that element Si in AgO-d hybrids still exists in the form of amorphous silica and cristobalite. Calcined diatomite exhibits a good chemical stability.

The Ag3d XPS spectrum of AgO-d hybrids is shown in Fig. 5. The high-resolution $Ag3d_{5/2}$ spectrum is resolved into two individual component peaks. This indicates element Ag in AgO-d hybrids exists in two forms. The peak at 368.1 eV is contributed to AgO [46], and the other peak at 367.7 eV is assigned as Ag_2O [47]. It is also found that 92.44% of element Ag exists in the form of AgO, and 7.56% in the form of Ag_2O in the silver compounds, indicating that most of absorbed Ag^{+} on diatomite can be oxidized to form AgO directly. This result further proves that there are a few of Ag_2O existing in AgO-d hybrids deduced from XRD analysis.

To further study the chemical binding state of element Ag in AgO-d hybrids, the Ag MNN Auger peak lines were analyzed in this work, as shown in Fig. 6. The Ag MNN Auger peak of AgO-d hybrids is resolved into two individual component peaks. The peaks at 351.2 eV and 356.6 eV are related to Ag_2O [48] and AgO [49], correspondingly. This confirms that element Ag in AgO-d hybrids exists in the form of AgO and Ag_2O.

3.4.3. FT-IR analysis

The chemical structures of calcined diatomite and AgO-d hybrids were analyzed by FT-IR in the range of 400–4000 cm^{-1}, as shown in Fig. 7. The peak locations relating to the corresponding chemical bonds are in a good agreement with those reported in the literatures [50–53]. The main absorption bands of calcined diatomite were found at 474.5, 613.4, 790.8, 1091.7, 1402.2, 1462.0, 1629.8, 1664.6, 2167.9 and 3450.6 cm^{-1}. The absorption peak at 474.5 cm^{-1} is attributed to the Si–O–Si bending vibration. The bands at 613.4 and 790.8 cm^{-1} represent SiO–H vibration. The band at 1091.7 cm^{-1} reflects the siloxane (–Si–O–Si–) group stretching, and the peak at

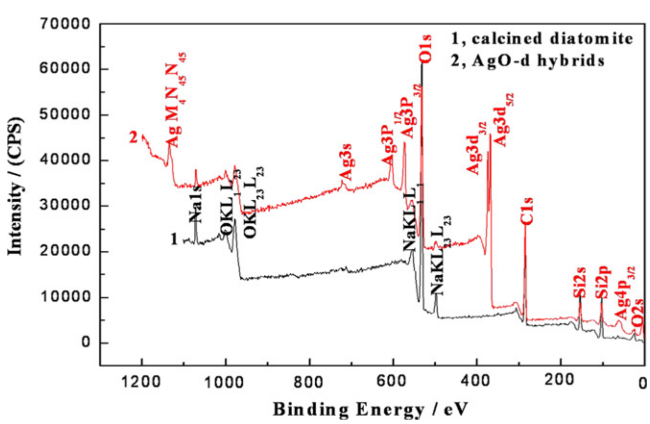

Fig. 3. XPS survey spectra of calcined diatomite and AgO-d hybrids obtained by oxidation of Ag^{+} adsorbed onto diatomite (immersing in $AgNO_3$ solution of 2.0 mol L^{-1}, $n(KOH)/n(AgNO_3)=7.5$, 333.15 K, 1.5 h).

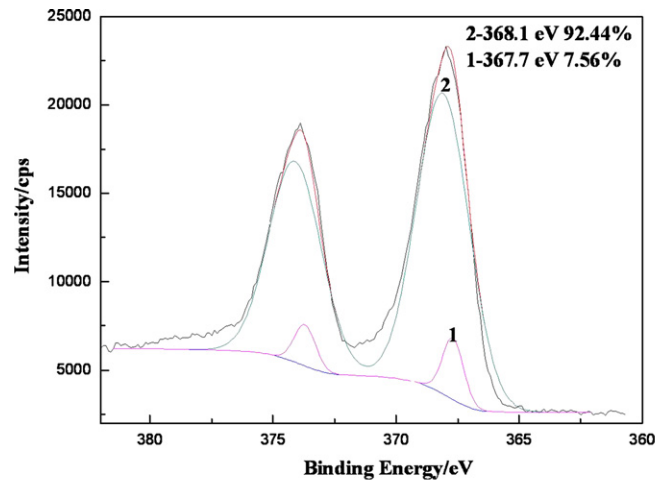

Fig. 5. XPS Ag3d spectrum for AgO-d hybrids obtained by oxidation of Ag^{+} adsorbed onto diatomite (immersing in $AgNO_3$ solution of 2.0 mol L^{-1}, $n(KOH)/n(AgNO_3)=7.5$, 333.15 K, 1.5 h).

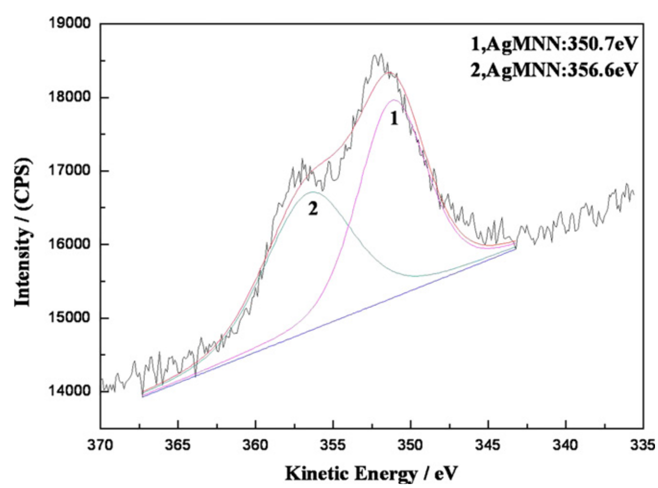

Fig. 6. Ag MNN Auger spectrum of AgO-d hybrids obtained by oxidation of Ag^{+} adsorbed onto diatomite (immersing in $AgNO_3$ solution of 2.0 mol L^{-1}, $n(KOH)/n(AgNO_3)=7.5$, 333.15 K, 1.5 h).

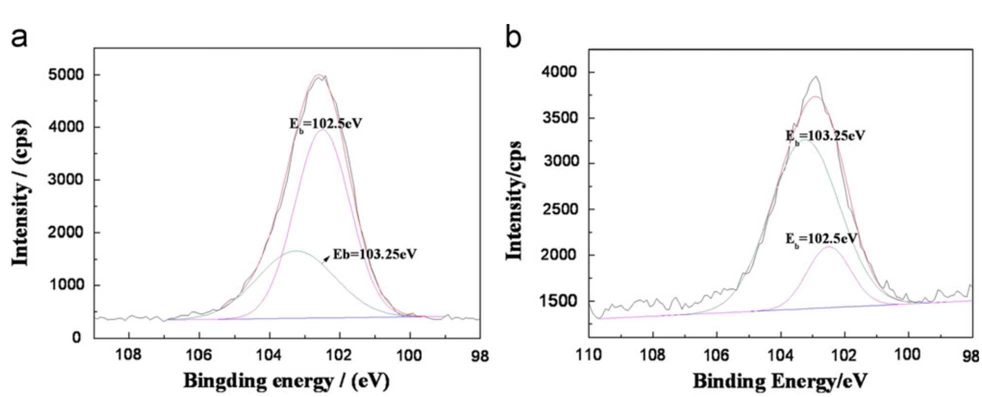

Fig. 4. XPS Si2p spectra for calcined diatomite and AgO-d hybrids obtained by oxidation of Ag^{+} adsorbed onto diatomite (immersing in $AgNO_3$ solution of 2.0 mol L^{-1}, $n(KOH)/n(AgNO_3)=7.5$, 333.15 K, 1.5 h). (a) calcined diatomite and (b) AgO-d hybrids.

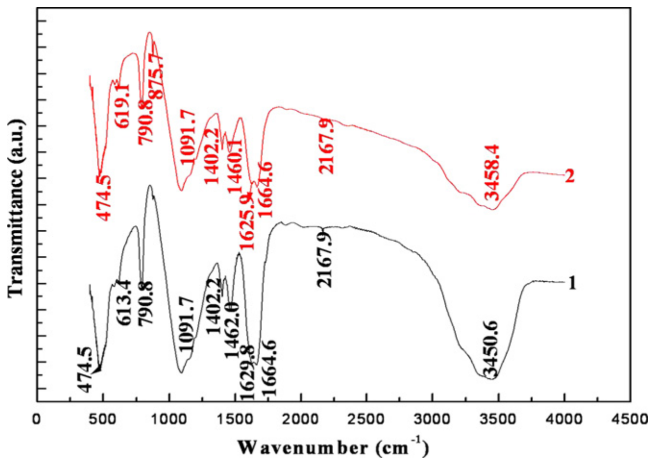

Fig. 7. Infrared absorption spectra of calcined diatomite and AgO-d hybrids obtained by oxidation of Ag^+ adsorbed onto diatomite (immersing in $AgNO_3$ solution of 2.0 mol L^{-1}, $n(KOH)/n(AgNO_3)=7.5$, 333.15 K, 1.5 h). (1) Calcined diatomite and (2) AgO-d hybrids.

2167.9 cm^{-1} is attributed to the Si–H stretching. The sharp bands observed at 1402.2 cm^{-1} and 1462.0 cm^{-1} are the characteristics of bending in-plane-OH vibrations or bending in-plane sym. The bands at 1629.8–1664.6 cm^{-1} represent H–O–H bonding vibration of water, and the intense and broad band at 3450.6 cm^{-1} can be assigned to O–H stretching vibrations in hydroxyl groups. This attributes to the presence of adsorbed water by diatomite samples. Compared with the spectrum of calcined diatomite, the peaks' positions of AgO-d hybrids had small shifts, which was associated with the chemical combination between calcined diatomite and AgO. The bands at 613.4, 1462.0, 1629.8 and 3450.6 cm^{-1} were shifted to 619.1, 1460.1, 1625.9 and 3458.4 cm^{-1} respectively. This could result from the interaction between AgO and SiO–H, –OH of diatomite in AgO-d hybrids.

There are two possible interactions between AgO and SiO–H, –OH of diatomite in AgO-d hybrids. Diatomite was immersed firstly in silver nitrate solution before the preparation of AgO-d hybrids. In nature, the most common medium diatomite contacted is water. Silicon hydroxylation function groups can be formed, after it hydroxylates in water according to Eqs. (5) and (6).

$$>Si+OH=\ >SiOH \tag{5}$$

$$>SiO+H=\ >SiOH \tag{6}$$

Hydroxylation function group can react with inorganic cations in solution through electrostatic interaction, which is called surface coordinate reaction [54]. Since there is empty orbital in silver ions, they have a strong tendency to coordinate. Thus, silver ions react with the hydroxylation function groups in water according to Eq. (7) and (8), and silver ions are absorbed.

$$>SiOH+Ag^{+}=\ >SiOAg+H^{+} \tag{7}$$

$$>SiOH+AgOH=\ >SiOAgOH^{-}+H^{+} \tag{8}$$

After the immersion, silver ions absorbed on diatomite were oxidized by potassium persulfate to form AgO-d hybrids, and the $>$SiOAgO or ($>$SiO–Ag–O)– bond was formed. Moreover, there are three stages of reactions when AgO-d hybrids were dried. The first stage is desorption of free water and bound water on the surfaces of diatomite. Desorption of divalent silver oxide hydrated water is the second stage. The third stage is dehydration between OH groups and then Si–O–Ag–O bonds were formed, combining AgO with diatomite together firmly. The reaction can be expressed as shown in Fig. 8.

3.5. Morphology analysis

Digital photographs of calcined diatomite and AgO-d hybrids are shown in Fig. 9. The color of diatomite changed from white to gray-black after chemical oxidation. It has been found that the color of silver nanoparticles is yellowish brown, those of Ag_2O nanoparticles and ultrafine AgO powders are brownish black and black respectively. Thus, the color of AgO-d hybrids might arise from the diffusion of submicron AgO particles or Ag_2O nanoparticles onto diatomite.

Fig. 10 shows the SEM micrographs of AgO-d hybrids. AgO-d hybrids were mainly composed of large particles with a thickness of ~2 μm and length of ~20 μm. Some lamelliform particles were diffused onto diatomite (Fig. 10(a)). Fig. 10(b) shows the image of the substance, which marked with circle 1 in Fig. 10(a). The substances were composed of a large number of lamelliform particles with a thickness around 0.05 μm. Compared with calcined diatomite (Fig. 1(b)), the morphology of AgO-d hybrids is changed after the chemical oxidation, and the discoid diatomite particles are crushed. Due to its strong adsorptive ability, diatomite adsorbs a certain amount of Ag^+. Consequently, the formation of AgO grains through the oxidation of Ag^+ by $S_2O_8^{2-}$ results in the volume expansion, leading to the breaking of diatomite particles.

EDS analysis was carried out to focus on the substance marked with circle 2 in Fig. 10(a), as shown in Fig. 11. There were most of element Ag, Si and O, whose atomic percentages were correspondingly 1.44%, 29.06% and 69.50%. This illustrates that element Ag is diffused into diatomite. Furthermore, the atomic ratio of 2.39 of O/Si exceeded the theoretical value of silica, 2. This confirms that silver may exist in the form of oxide.

3.6. Bactericidal effects

Fig. 12 shows the germicidal effects of AgO-d hybrids with different concentrations (10, 30, 70, and 112 mg L^{-1}) against *S. aureus* and *E. coli*. The bactericidal rates were over 99.9% against both *S. aureus* and *E. coli*, exhibiting a good germicidal effect. When the concentration of the

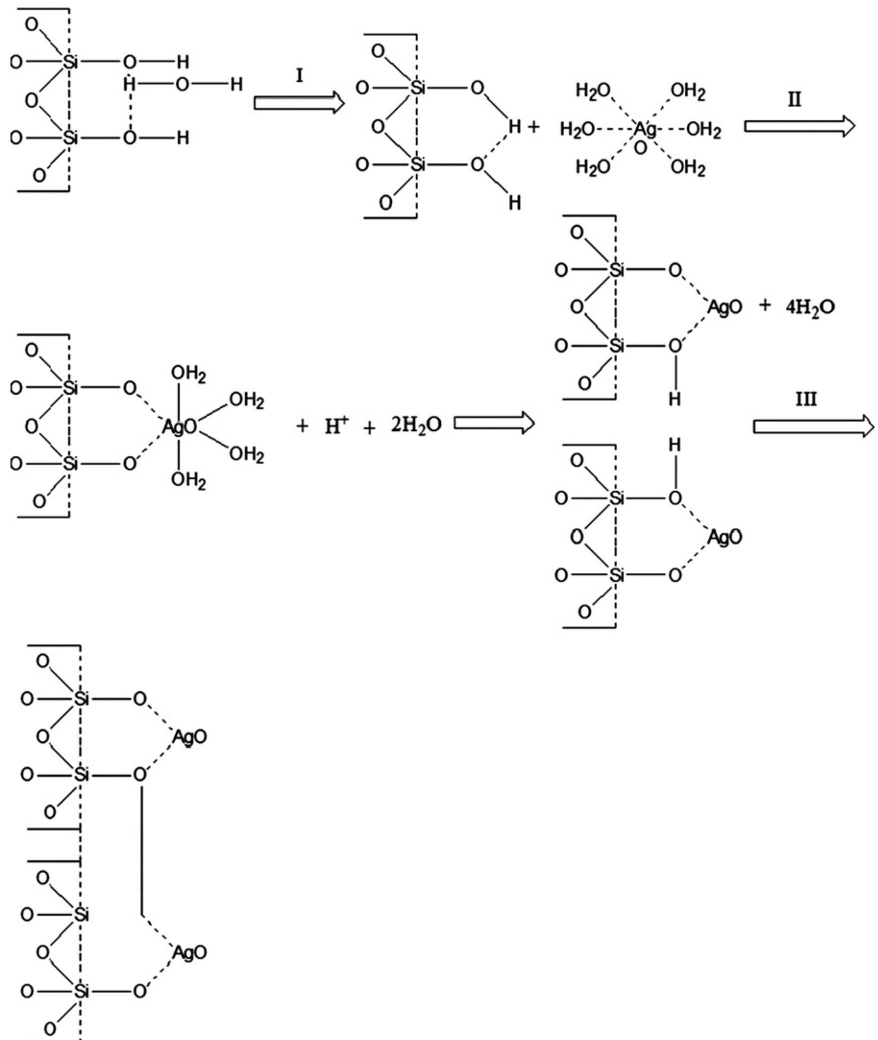

Fig. 8. Schematic diagram of reaction mechanism of diatomite solidifying AgO.

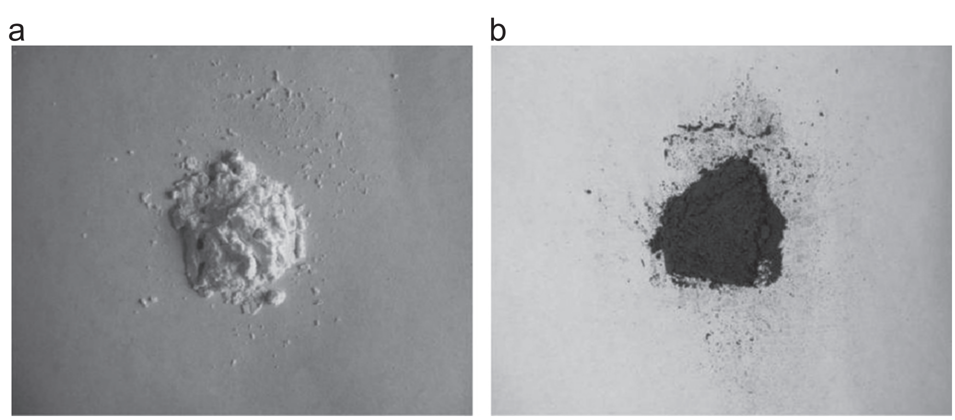

Fig. 9. Digital photographs of calcined diatomite (a) and AgO-d hybrids obtained by oxidation of Ag^+ adsorbed onto diatomite (immersing in $AgNO_3$ solution of 2.0 mol L^{-1}, $n(KOH)/n(AgNO_3)=7.5$, 333.15 K, 1.5 h) (b).

AgO-d hybrids solution was 10 mg L^{-1} and the sterilization time was 30 min, 99.974% of *S. aureus* and 99.944% of *E. coli* were killed. For the same sterilization time, the bactericidal rates were enhanced with the concentration of AgO-d hybrids. When the concentration was up to 112 mg L^{-1}, the germicidal rates of AgO-d hybrids against *S. aureus* and *E. coli* rose to 99.987% and 99.981% respectively. The germicidal rates are improved by 0.013% and 0.037%

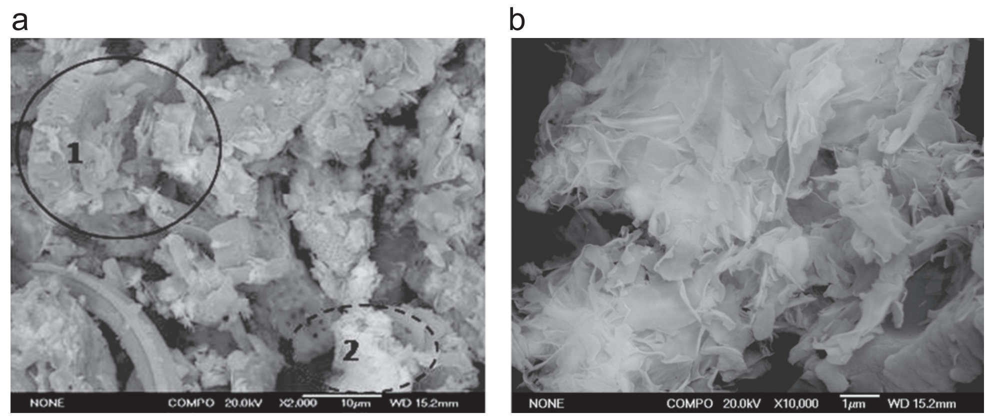

Fig. 10. SEM morphologies of AgO-d hybrids obtained by oxidation of Ag^{+} adsorbed onto diatomite (immersing in $AgNO_3$ solution of 2.0 mol L^{-1}, $n(KOH)/n(AgNO_3)=7.5$, 333.15 K, 1.5 h) (a) 2000 times and (b) 10,000 times.

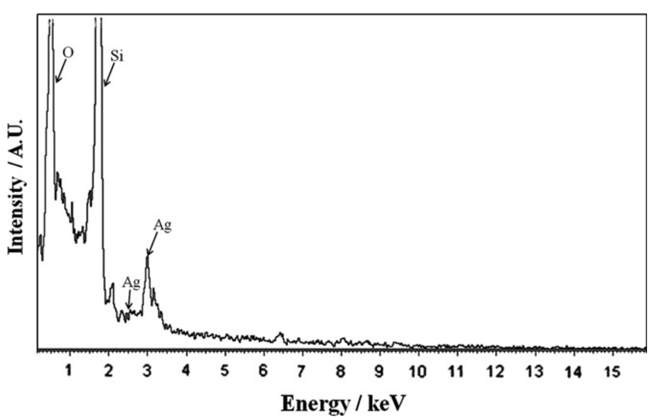

Fig. 11. Local EDS analysis result of AgO-d hybrids obtained by oxidation of Ag^{+} adsorbed onto diatomite (immersing in $AgNO_3$ solution of 2.0 mol L^{-1}, $n(KOH)/n(AgNO_3)=7.5$, 333.15 K, 1.5 h).

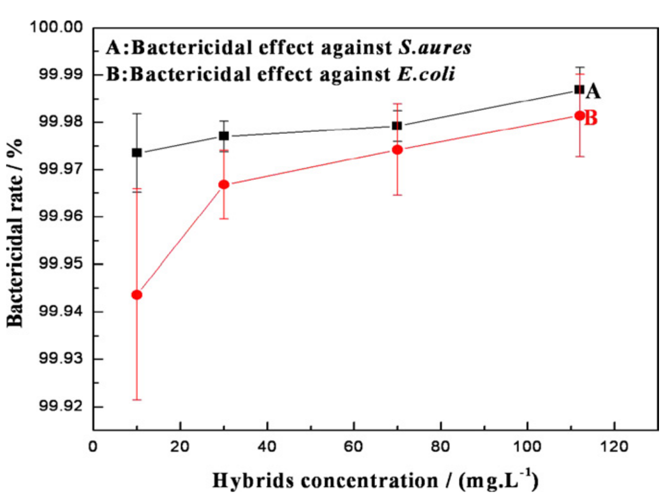

Fig. 12. Bactericidal effects for AgO-d hybrids with different concentrations against *S. aureus* and *E. coli*.

correspondingly, which forms a comparison to AgO-d hybrids with a concentration of 10 mg L^{-1}. This indicates that high efficient sterilization effect can be achieved by using trace AgO-d hybrids. There are two possible reasons why AgO-d hybrids have the bactericidal activity. One is that bacteria are easily adsorbed onto AgO particles, and the Ag^{2+} released from AgO changes the permeability of cell wall, denaturates protein, inactivates enzyme, leading to the lysis and death of the cells. The other is that the remaining of AgO particles in AgO-d hybrids solution or dissolved Ag^{2+} may inhibit the replicative capacity of cell and affect the growth of bacteria.

4. Conclusions

(1) AgO-d hybrids with high AgO content were directly synthesized by chemical oxidation, using silver nitrate and calcined diatomite as raw materials, potassium persulfate as oxidant. The optimum preparing parameters for AgO-d hybrids were as follows: initial reaction temperature of 333.15 K, silver nitrate concentration of 2.0 mol L^{-1}, $n(KOH)/n(AgNO_3)$ value of 7.5 and reaction time of 1.5 h. The AgO content of AgO-d hybrids obtained with optimum preparing parameters reached to 20.8%, and the median particle size, size distribution were 18.53 μm and 0.614–116.5 μm respectively. Element Ag can be released from AgO-d hybrids in water solution, with a releasing rate of around 3.20×10^{-2} mg $(L\ h)^{-1}$.

(2) Calcined diatomite was composed of amorphous SiO_2 and tetragonal low cristobalite. After the deposition of AgO, AgO-d hybrids were composed of amorphous SiO_2, tetragonal low cristobalite, monoclinic AgO and a few of cubic Ag_2O. The deposition of silver oxides on diatomite did not change the phase composition and crystal structure of diatomite.

(3) AgO-d hybrids exhibited a strong sterilization activity. When the concentration of AgO-d hybrids was 10 mg L^{-1} and the sterilization time was 30 min, the germicidal rates of AgO-d hybrids against *S. aureus* and *E. coli* reached up to 99.970% and 99.941% respectively. This result would be of great importance in expanding use of the bactericidal hybrids in many other applications that require strong bactericidal activity.

Acknowledgments

This work was supported financially by Science and Technology Planning Project of Xi'an, Special Research Project of Education Department of Shaanxi Province of China and Excellent Doctor Degree Dissertation Research Foundation of Xi'an University of Technology. The authors acknowledge Professor Weiwei Wang at Northwest University for his assistance in the antimicrobial test.

References

[1] K.H. Cho, J.E. Park, T. Osaka, S.G. Park, The study of antimicrobial activity and preservative effects of nanosilver ingredient, Electrochimica Acta 51 (2005) 956–960.
[2] V. Shashikala, V. Siva Kumar, A.H. Padmasri, B. David Raju, S. Venkata Mohau, P. Nageswara Sarma, K.S. Rama Rao, Advantages of nano-silver-carbon covered alumina catalyst prepared by electro-chemical method for drinking water purification, Journal of Molecular Catalysis A: Chemical 268 (2007) 95–100.
[3] K. Xu, J.X. Wang, X.L. Kang, J.F. Chen, Fabrication of antibacterial monodispersed Ag–SiO_2 core-shell nanoparticles with high concentration, Materials Letters 63 (2009) 31–33.
[4] I. Sondi, B. Salopek-Sondi, Silver nanoparticles as antimicrobial agent: a case study on *E. coli* as a model for Gram-negative bacteria, Journal of Colloid and Interface Science 275 (2004) 177–182.
[5] A.T. Le, P.T. Huy, P.D. Tam, T.Q. Huy, P.D. Cam, A.A. Kudrinskiy, A. Krutyakov, Green synthesis of finely-dispersed highly bactericidal silver nanoparticles via modified Tollens technique, Current Applied Physics 10 (2010) 910–916.
[6] B. Thati, A. Noble, R. Rowan, B.S. Creaven, M. Walsh, M. McCann, D. Egan, K. Kavanagh, Mechanism of action of coumarin and silver(I)-coumarin complexes against the pathogenic yeast *Candida albicans*, Toxicology in Vitro 21 (2007) 801–808.
[7] D.C. Tien, K.H. Tseng, C.Y. Liao, T.T. Tsung, Colloidal silver fabrication using the spark discharge system and its antimicrobial effect on *Staphylococcus aureus*, Medical Engineering & Physics 30 (2008) 948–952.
[8] T. Yuranova, A.G. Rincon, C. Pulgarin, D. Laub, N. Xantopoulos, H.J. Mathieu, J. Kiwi, Performance and characterization of Ag-cotton and Ag/TiO_2 loaded textiles during the abatement of *E. coli*, Journal of Photochemistry and Photobiology A: Chemistry 181 (2006) 363–369.
[9] C.M. Betbeze, C.C. Wu, S.G. Krohne, J. Stiles, In vitro fungistatic and fungicidal activities of silver sulfadiazine and natamycin on pathogenic fungi isolated from horses with keratomy cosis, American Journal of Veterinary Research 67 (2006) 1788–1793.
[10] A. Panacek, M. Kolar, R. Vecerova, R. Prucek, J. Soukupova, V. Krystof, P. Hamal, R. Zboril, L. Kvitek, Antifungal activity of silver nanoparticles against *Candida spp*., Biomaterials 30 (2009) 6333–6340.
[11] A. Kathiravan, R. Renganathan, S. Anandan, Interaction of colloidal AgTiO_2 nanoparticles with bovine serum albumin, Polyhedron 28 (2009) 157–161.
[12] J.L. Elechiguerra, J.L. Burt, J.R. Morones, A. Camacho-Bragado, X.X. Gao, H.H. Lara, M.J. Yacaman, Interaction of silver nanoparticles with HIV-1, Journal of Nanobiotechnology 3 (2005) 1–10.
[13] S.S. Mahapatra, N. Karak, Silver nanoparticle in hyperbranched polyamine: Synthesis, characterization and antibacterial activity, Materials Chemistry and Physics 112 (2008) 1114–1119.
[14] F. Mirzajani, A. Ghassempour, A. Aliahmadi, M.A. Esmaeili, Antibacterial effect of silver nanoparticles on *Staphylococcus aureus*, Research in Microbiology 162 (2011) 542–549.
[15] Z.Z. Li, L.J. Fan, T. Zhang, K. Li, Facile synthesis of Ag nanoparticles supported on MWCNTs with favorable stability and their bactericidal properties, Journal of Hazardous Materials 187 (2011) 466–472.
[16] M. Sathishkumar, K. Sneha, Y.S. Yun, Immobilization of silver nanoparticles synthesized using *Curcuma longa* tuber powder and extract on cotton cloth for bactericidal activity, Bioresource Technology 101 (2010) 7958–7965.
[17] D. Gangadharan, K. Harshvardan, G. Gnanasekar, D. Dixit, K.M. Popat, P.S. Anand, Polymeric microspheres containing silver nanoparticles as a bactericidal agent for water disinfection, Water Research 44 (2010) 5481–5487.
[18] A.M. El-Kady, A.F. Ali, R.A. Rizk, M.M. Ahmed, Synthesis, characterization and microbiological response of silver doped bioactive glass nanoparticles, Ceramics International 38 (2012) 177–188.
[19] A.A. Ahmed, A.A. Ali, D.A.R. Mahmoud, A.M. Elifiqi, Study on the preparation and properties of silver-doped phosphate antibacterial glasses, Solid State Sciences 13 (2011) 981–992.
[20] I.D.L. Rosa-Gomez, M.T. Olguin, D. Alcantara, Antibacterial behavior of silver-modified clinoptilolite-heulandite rich tuff on coliform microorganisms from wastewater in a column system, Journal of Environmental Management 88 (2008) 853–863.
[21] D. Dellasega, A. Facibeni, F.D. Fonzo, V. Russo, C. Conti, C. Ducati, C.S. Casari, A.L.I. Bassi, C.E. Bottani, Nanostructured high valence silver oxide produced by pulsed laser deposition, Applied Surface Science 255 (2010) 5248–5251.
[22] N.C. Kasuga, R. Yamamoto, A. Hara, A. Amano, K. Nomiya, Molecular design, crystal structure, molecular design, crystal structure, antimicrobial activity and reactivity of light-stable and water-soluble Ag-O bonding silver(I) complexes, dinuclear silver(I) N-acetylglycinate, Inorganica Chimica Acta 359 (2006) 4412–4416.
[23] Y.N. Li, Y.Z. Sun, Y.S. Zhang, L.P. Du, Y. Sun, Q.H. He, Antibacterial property of Ag_2O films vacuum-deposited on high density polyethylene substrates, Chinese Journal of Vacuum Science and Technology 31 (2011) 129–133 (in Chinese).
[24] W.N. Shen, L.J. Feng, H. Feng, Z.Z. Kong, M.J. Guo, Ultrafine silver(II) oxide particles decorated porous ceramic composites for water treatment, Chemical Engineering Journal 175 (2011) 592–599.
[25] E. Ülkür, O. Oncul, H. Karagoz, E. Yeniz, B. Celiköz, Comparison of silver-coated dressing (Acticoat^{TM}), chlorhexidine acetate 0.5% (Bactigrass), and fusidic acid 2% (Fucidin), Burns 31 (2005) 874–877.
[26] V. Alt, T. Bechert, P. SteinrÜcke, M. Wagener, P. Seidel, E. Dingeldein, E. Domann, R. Schnettler, An in vitro assessment of the antibacterial properties and cytotoxicity of nanoparticulate silver bone cement, Biomaterials 25 (2004) 4383–4391.
[27] G. Gosheger, J. Hardes, H. Ahrens, A. Streitburger, H. Buerger, M. Erren, A. Gunsel, F.H. Kemper, W. Winkelmann, C.V. Eiff, Silver-coated megaendoprostheses in a rabbit model-an analysis of the infection rate and toxicological side effects, Biomaterials 25 (2004) 5547–5556.
[28] M.E. Rupp, T. Fitzgerald, N. Marion, V. Helget, S. Puumala, J.R. Anderson, Effect of silver-coated urinary catheters: efficacy, cost-effectiveness, and antimicrobial resistance, American Journal of Infection Control 32 (2004) 445–450.
[29] H.J. Lee, S.H. Jeong, Bacteriosis and skin innoxiousness of nanosize silver colloids on textile, Textile Research Journal 75 (2005) 551–556.
[30] M.S. Antelman, Divalent silver oxide bactericides, United States Patent US005098582A.
[31] W.N. Shen, L.J. Feng, Z.Z. Kong, H. Feng, Ultrafine silver peroxide powders prepared by ozone oxidization method and its antibacterial property, Acta Chimica Sinica 69 (2011) 277–283 (in Chinese).
[32] P. Lalueza, M. Monzon, M. Arruebo, J. Santamaria, Bactericidal effects of different silver-containing materials, Materials Research Bulletin 46 (2011) 2070–2076.
[33] Q. Li, K. Chen, L.L. Jiao, G.G. Zhou, The preparation of the dispersed liquid of nanometer bivalent silver oxide, Water Purification Technology 27 (2008) 12–15 in Chinese.
[34] Y.H. Kim, D.K. Lee, H.G. Cha, C.W. Kim, Y.S. Kang, Synthesis and characterization of antibacterial Ag–SiO_2 nanocomposite, Journal of Physical Chemistry C 111 (2007) 3629–3635.

[35] M.A.M. Khraisheh, Y.S. Al-degs, W.A.M. Mcminn, Remediation of wastewater containing heavy metals using raw and modified diatomite, Chemical Engineering Journal 99 (2004) 177–184.
[36] M.A. Al-Ghouti, M.A.M. Khraisheh, M. Tutuji, Flow injection potentiometric stripping analysis for study of adsorption of heavy metal ions onto modified diatomite, Chemical Engineering Journal 104 (2004) 83–91.
[37] Y.X. Jia, W. Han, G.X. Xiong, W.S. Yang, Layer-by-layer assembly of TiO_2 colloids onto diatomite to build hierarchical porous materials, Journal of Colloid and Interface Science 323 (2008) 326–331.
[38] E. Rossetto, D.I. Petkowicz, J.H.Z.D. Santos, S.B.C. Pergher, F.G. Penha, Bentonites impregnated with TiO_2 for photodegradation of methylene blue, Applied Clay Science 48 (2010) 602–606.
[39] S.K. Rastogi, V.J. Rutledge, C. Gibson, D.A. Newcombe, J.R. Branen, A.L. Branen, Ag colloids and Ag clusters over EDAPTMS-coated silica nanoparticles: synthesis, characterization, and antibacterial activity against *Escherichia coli*, Nanomedicine: Nanotechnology, Biology and Medicine 7 (2011) 305–314.
[40] B.G. Huang, G.H. Xiao, Study on assay method of silver peroxide, Gold 13 (1992) 54–57 (in Chinese).
[41] Y.Y. Dong, F.Y. Zhang, Y. Wang, Inorganic and analytical chemistry, second ed., Science Press, Beijing, 2005.
[42] S.L. Zhan, J.X. Lin, M.H. Fang, X.Q. Qian, Preparation of manganese oxides-modified diatomite and its adsorption performance for dyes, Rare Metal Materials and Engineering 39 (2010) 397–400.
[43] M.S. Antelman, Method of treating water employing tetrasilver tetroxide crystals, United States Patent US005211855A.
[44] T.L. Barr, An esca study of termination of the passivation of elemental metals, Journal of Physical Chemistry 82 (1978) 1801–1810.
[45] C.D. Wagner, J.F. Moulder, L.E. Davis, W.M. Riggs, in: Handbook of X-Ray Photoelectron Spectroscopy, Perking–Elmer Corporation Physical Electronics Division, Minnesota, 1979.
[46] L.J. Gerenser, Photoemission investigation of silver/poly(ethylene terephthalate) interfacial chemistry: the effect of oxygen-plasma treatment, Journal of Vacuum Science & Technology A 8 (1990) 3682–3691.
[47] J.S. Hammond, S.W. Gaarenstroom, N. Winograd, X-ray photoelectron spectroscopic studies of cadmium and silver-oxygen surface, Analytical Chemistry 47 (1975) 2193–2199.
[48] L.H. Tjeng, M.B.J. Meinders, J.V. Elp, J. Ghijsen, G.A. Sawatzky, R.L. Johnson, Electronic structure of Ag_2O, Physical Review B 41 (1990) 3190.
[49] D. Briggs, M.P. Seah, Practical Surface Analysis: By Auger and X-Ray Photo-Electron Spectroscopy, John Willey & Sons, Hoboken, 1993.
[50] Y.B. Zeng, J. Park, Characterization and coagulation performance of a novel inorganic polymer coagulant-poly-zinc-silicate–sulfate, Colloids and Surfaces A: Physicochemical and Engineering Aspects 334 (2009) 147–154.
[51] M. Sprynskyy, I. Kovalchuk, B. Buszewski, The separation of uranium ions by natural and modified diatomite from aqueous solution, Journal of Hazardous Materials 181 (2010) 700–707.
[52] C.L. Wang, J.T. Yan, X.J. Cui, H.Y. Wang, Synthesis of raspberry-like monodisperse magnetic hollow hybrid nanospheres by coating polystyrene template with $Fe_3O_4@SiO_2$ particles, Journal of Colloid and Interface Science 354 (2011) 94–99.
[53] P. Bankovic, N.R. Demarquette, M.L.P.D. Silva, Obtention of selective membranes for water and hydrophobic liquids by plasma enhanced chemical vapor deposition on porous substrates, Materials Science and Engineering: B 112 (2004) 165–170.
[54] N. Liang, H. Ding, Y.T. Hu, B.K. W, Reaction mechanism between Zn^{2+} and diatomite in preparation of Zn^{2+}/diatomite antibacterial agent, Materials Science Forum 685 (2011) 260–263.